JTTEE5 20:358–365
DOI: 10.1007/s11666-010-9558-0
1059-9630/$19.00 © ASM International

Thermophysical and Microstructural Studies on Thermally Sprayed Tungsten Carbide-Cobalt Coatings

Sven Thiele, Kerstin Sempf, Klaus Jaenicke-Roessler, Lutz-Michael Berger, and Jörg Spatzier

(Submitted May 21, 2010; in revised form August 25, 2010)

The development of new hardmetal coating applications such as fatigue-loaded parts, structural components, and tools for metal forming is connected with improvement of their performance and reliability. For modelling purposes, the knowledge of thermophysical, mechanical, and other material data is required. However, this information is still missing today. In this study, the thermophysical data of a WC-17Co coating sprayed with a liquid-fuelled HVOF-process from a commercial agglomerated and sintered feedstock powder from room temperature up to 700 °C was determined as an example. The dependence of the heat conductivity on temperature was obtained through measurement of the coefficient of thermal expansion, the specific heat capacity, and the thermal diffusivity. Heat conductivities ranging from 29.2 W/(mK) at 50 °C to 35.4 W/(mK) at 700 °C were determined. All measurements were performed twice (as-sprayed and after the first thermal cycle) to take into account the structural and compositional changes. Extensive XRD and FESEM studies were performed to characterize the phase compositions and microstructures in the as-sprayed and heat-treated states. Bulk samples obtained by spark plasma sintering from the feedstock powder were studied for comparison.

Keywords nanostructured coatings, thermal and phase stability of coatings, thermal cycling

1. Introduction

Thermally sprayed hardmetal coatings are commonly used for protection against abrasion and erosion. Based on earlier studies, e.g., by Ahmed and Hadfield (Ref 1), it was recently confirmed that these coatings can be used for fatigue-loaded tools for metal-forming and structural components with high contact loads in service conditions such as gear wheels or camshafts (Ref 2). Progress in increasing durability and reliability was made through the application of the state-of-the-art high velocity oxy-fuel (HVOF) spray process and the development of new tailored feedstock materials for coating deposition. The development of these applications also requires the use of modelling. Unfortunately, there is a significant lack of reliable thermophysical and mechanical data for thermal spray coatings to be used for modelling purposes.

When compared with bulk materials, thermal spray coatings having the same nominal compositions are characterized by a much broader range of properties (Ref 3, 4). This is due to the specific preparation conditions, characterized by the use of different types of feedstock powders, spray processes, and spray parameters. For this reason it is especially important that detailed structural investigations will be performed in conjunction with determination of the thermophysical or mechanical properties.

The chemical and phase compositions of WC-Co coatings depend on the spray process and the characteristics of the feedstock powder. The feedstock powder undergoes decomposition and decarburization reactions during the spray process.

The decomposition and oxidation of WC-Co during spraying is usually analyzed in terms of the three-step mechanism originally proposed by Vinayo et al. (Ref 5) for APS of WC-Co:

$$2WC \rightarrow W_2C + C \quad \text{(Eq 1)}$$

$$W_2C + {}^1/_2O_2 \rightarrow W_2(C,O) \quad \text{(Eq 2)}$$

$$W_2(C,O) \rightarrow 2W + CO \quad \text{(Eq 3)}$$

Although formulated as a hypothesis by Vinayo et al. (Ref 5), in numerous later citations these reactions have tended to be treated as an experimentally verified fact (Ref 4) and were also used to describe the decomposition reactions in HVOF-sprayed coatings, e.g., by

This article is an invited paper selected from presentations at the 2010 International Thermal Spray Conference and has been expanded from the original presentation. It is simultaneously published in *Thermal Spray: Global Solutions for Future Applications, Proceedings of the 2010 International Thermal Spray Conference*, Singapore, May 3-5, 2010, Basil R. Marple, Arvind Agarwal, Margaret M. Hyland, Yuk-Chiu Lau, Chang-Jiu Li, Rogerio S. Lima, and Ghislain Montavon, Ed., ASM International, Materials Park, OH, 2011.

Sven Thiele, Kerstin Sempf, and **Klaus Jaenicke-Roessler**, Fraunhofer Institute IKTS, Dresden, Germany; and **Lutz-Michael Berger** and **Jörg Spatzier**, Fraunhofer Institute IWS, Dresden, Germany. Contact e-mail: Sven.Thiele@ikts.fraunhofer.de.

Guilemany et al. (Ref 6). W_2C is very often described as a phase present in HVOF-sprayed coatings (Ref 6-12). It is described to be located in HVOF-sprayed coatings in rims around WC grains by several authors (Ref 6, 9, 10, 12). Except in the study of Vinayo et al. (Ref 5) only Li et al. (Ref 7) mention the existence of $W_2(C,O)$ in plasma-sprayed coatings. Metallic tungsten is also often observed in WC-Co coatings sprayed by APS, detonation gun spraying (DGS) and HVOF, when intensive degradation occurs (Ref 5, 9, 10, 13).

Besides the processes during spraying, it is well known that due to the high cooling rates during deposition as-sprayed hardmetal coatings are in a nonequilibrium state. Both W_2C and metallic tungsten are characteristic phases for deposits in a nonequilibrium state. Heating in inert atmosphere above 600 °C leads to structural changes, bringing the phase composition closer to the equilibrium state (Ref 8, 10, 11, 14). The M_6C and $M_{12}C$, the so-called η-phases, are the possible equilibrium phases in the W-C-Co system, after loss of carbon in the spray process. Sometimes, their existence in as-sprayed coatings is also reported, e.g., (Ref 7, 8).

It should be also mentioned that the oxygen content in WC-Co coatings is very small. Values <0.2 wt.% (Ref 10, 15) and ~0.5 wt.% (Ref 16) have been reported. Low oxide scale adhesion strengths and, possibly, the high volatility of WO_3 seem to be responsible for this (Ref 16). A low oxygen content is important, due to reduction reactions and formation of gases which will occur in heating.

All structural and compositional changes must be taken into account for high-temperature applications. Among thermophysical coating properties, the heat conductivity λ is of great importance for the development of high-temperature applications. This property was not measured directly; it was calculated according to Eq 4

$$\lambda(T) = a(T) * C_p(T) * \rho(T) \quad \text{(Eq 4)}$$

where a is the thermal diffusivity, C_p is the specific heat capacity, and ρ is the density, calculated from the coefficient of thermal expansion $\alpha(T)$ and the room temperature density $\rho_0(RT)$.

Three different thermophysical measurements are necessary: the coefficient of thermal expansion (CTE) obtained by dilatometry, the specific heat capacity obtained by differential scanning calorimetry (DSC), and thermal diffusivity obtained by laser flash method. In addition, sample preparation is laborious, since each measurement requires the preparation of special samples, free of the substrate materials. In addition, the CTE is also of importance for modelling internal stresses (Ref 11).

In this article, we have determined the dependence of the heat conductivity on temperature in the range from 50 to 700 °C for a WC-17Co coating. To the authors knowledge values for the heat conductivity of WC-Co coatings are not available in the literature. Two heating cycles were performed for all measurements to study the influence of the microstructural changes occurring as a result of the first cycle to be investigated. To calculate the heat conductivity the data from second heating cycles were used. The results of the thermoanalytical studies are discussed together with results of detailed microstructural studies.

2. Experimental

2.1 Thermal Spraying

An agglomerated and sintered WC-17 mass% Co feedstock powder (Amperit 527.074, H.C. Starck GmbH, Goslar, Germany) was selected for this study. The low-magnification micrograph (BSE mode) in Fig. 1a shows the microstructure of a feedstock powder particle. It shows the typical isomorphous shape containing a high amount of pores. The WC grains and the homogeneously distributed cobalt binder phase of this particle are shown in Fig. 1b. The XRD pattern of the feedstock powder is given below together with the pattern of the SPS bulk sample in Fig. 13.

Thermal spraying was performed with an HVOF process using a robot-handled paraffin-fuelled system (K2, GTVmbH, Luckenbach, Germany). All coatings were deposited on flat low-carbon steel substrates (S235) of dimensions 100 × 60 × 4 mm. The substrates were grit-blasted immediately before spraying. A powder feed rate

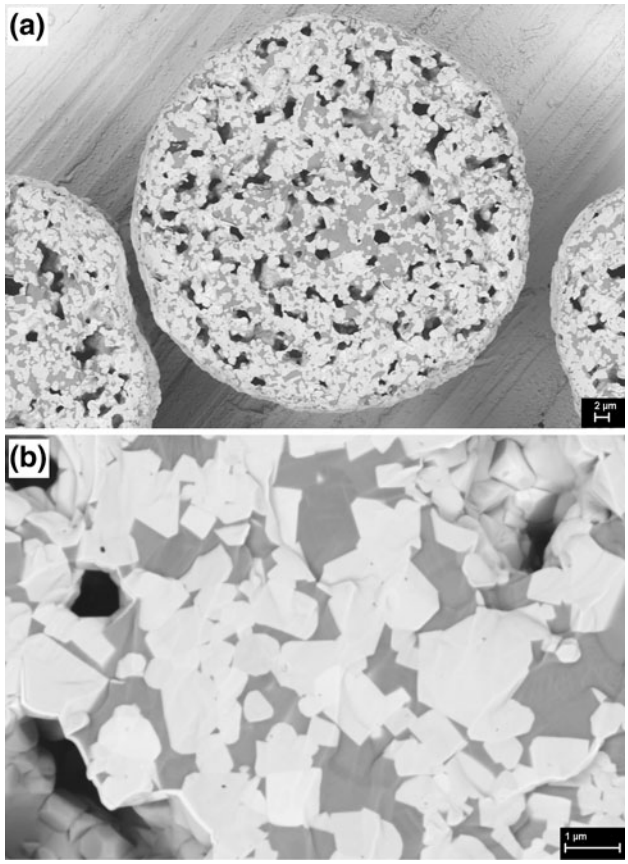

Fig. 1 Microstructure of a feedstock powder particle (BSE mode), (a) low magnification, (b) high-magnification

of 100 g/min, a value of lambda of 0.85, and a spray distance of 345 mm were applied. The traverse speed was 90 m/min and the resulting thickness per pass was about 12 μm. The surface temperature was kept below 220 °C. Direct cooling of the sample by compressed air and concurrent cooling of the sample holder was applied. The coating thickness was about 1400 μm due to test specimen size requirements. After the sample surfaces were ground the coatings were separated from the substrate and cut into the required dimensions for the different thermoanalytical measurements using electrical discharge machining (EDM).

2.2 Characterization

The following devices (all from Netzsch Gerätebau GmbH, Munich, Germany) were employed for the thermoanalytical measurements:

- thermal diffusivity $a(T)$: Laserflash Device LFA-427;
- CTE $\alpha(T)$: Thermomechanical Analysator TMA-402;
- specific heat capacity $C_p(T)$: Differential Scanning Calorimeter DSC 404.

All measurements were performed up to 700 °C in an argon atmosphere with the exception of the CTE which was measured in a helium atmosphere. Heating and cooling rates of 2 K/min and no dwell time at 700 °C were applied. Two thermal cycles were performed for all measurements except the CTE measurement where three cycles were carried out. While in atmospheric conditions WC-Co coatings oxidize intensively at temperatures above 600 °C (Ref 3, 4, 17), the coatings can serve in inert conditions at higher temperatures. Since all thermoanalytical measurements were performed in inert atmosphere, 700 °C was selected as the upper test temperature.

The density $\rho(T)$ is determined from the room temperature density $\rho(RT)$ and the thermal expansion coefficient $\alpha(T)$, while the thermal conductivity $\lambda(T)$ is calculated as a product of thermal diffusivity $a(T)$, density $\rho(T)$, and specific heat capacity $C_p(T)$.

In order to determine the phase composition, x-ray diffraction (XRD) was performed using monochromatic Cu Kα radiation with a XRD7 diffractometer (GE). The measurements were performed at the surfaces of samples used for thermoanalytical measurements, i.e., from the inner structure of the original coating. It was ensured that the heat-affected zone from EDM machining was removed by grinding. In addition, measurements on the original as-sprayed surface were performed. Cross sections of the coatings were prepared by mounting samples in resin, grinding, and polishing to a 0.25 μm finish. The cross sections were examined in a field emission scanning electron microscopy (FESEM, Zeiss NVision 40) using SE2 (secondary electrons), BSE (back-scattered electrons), and InLens and EBSD (electron backscatter diffraction) detectors. An EDX system (Oxford) was used to perform elemental mapping and to estimate the elemental composition at different spots.

To compare the microstructures of the coatings with that of a dense bulk material the WC-17Co feedstock powder was compacted by spark plasma sintering (SPS) using an HPD 25/1 (FCT, Sonneberg, Germany) device. The sample was heat-treated at 1250 °C for 5 min at a pressure of 30 MPa. The density of the sample was 99.1% of the theoretical density.

3. Results

3.1 Thermophysical Measurements

Figure 2, 3, and 4 show the results of measurements of specific heat capacity, CTE, and thermal diffusivity, respectively. As expected the plots of the first cycle differ significantly from those of the second cycles. In the CTE measurement three cycles were performed. Since only slight differences were found between the curves of the second and the third cycle at low temperatures all other measurements were limited to two cycles.

The complete results of the thermoanalytical measurements are compiled in Table 1.

3.2 Microstructures and Phase Compositions of the Coatings

Figure 5 shows XRD pattern of the sample in the as-sprayed state and after the second thermal cycle in the thermoanalytical equipment. Contrary to expectations, in the as-sprayed state the $M_{12}C$ (W_6Co_6C) and M_6C (W_3Co_3C) phases were found, whereas neither W_2C nor metallic tungsten or cobalt could be detected clearly.

As indicated by the broad halo around the peaks of the $M_{12}C$ phase, it is likely that tungsten, cobalt, and carbon

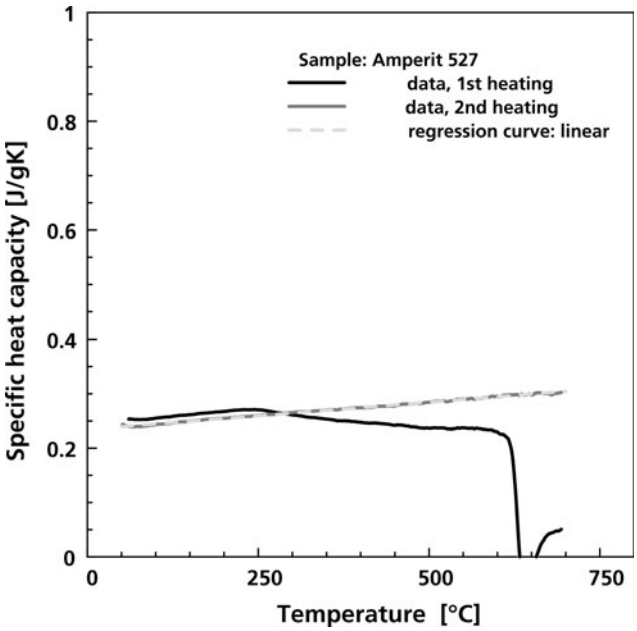

Fig. 2 Plots of the specific heat capacity vs. temperature

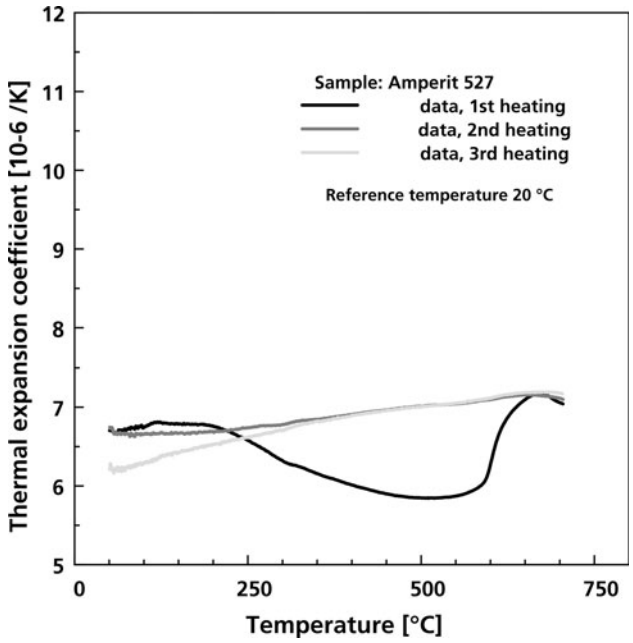

Fig. 3 Plots of the CTE vs. temperature

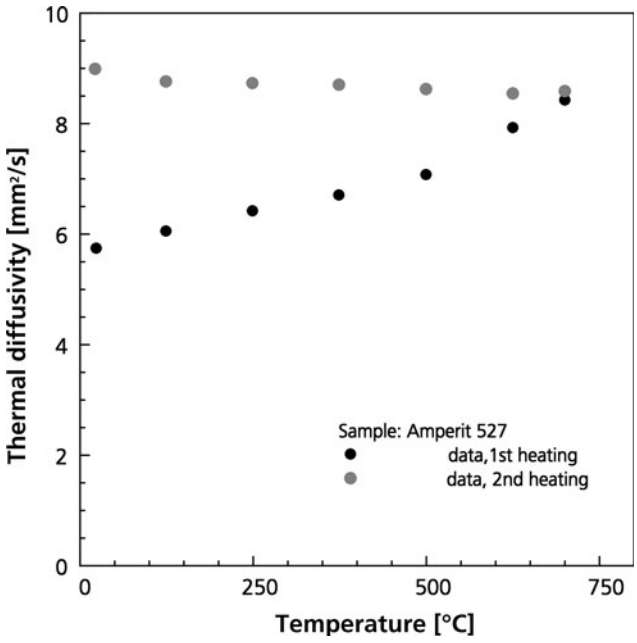

Fig. 4 Plots of the thermal diffusivity vs. temperature

Table 1 Thermophysical data of WC-17Co coatings

Temperature, °C	Coefficient of thermal expansion, 10^{-6}/K	Density, g/cm^3	Specific heat capacity, J/(g K)	Thermal diffusivity, mm^2/s	Thermal conductivity, W/(m K)
50	6.61	13.64	0.239	8.92	29.2
100	6.65	13.63	0.244	8.86	29.5
200	6.72	13.60	0.254	8.77	30.4
300	6.80	13.57	0.264	8.72	31.3
400	6.89	13.54	0.275	8.70	32.4
500	6.99	13.51	0.285	8.69	33.4
600	7.09	13.48	0.295	8.68	34.4
700	7.20	13.45	0.305	8.64	35.4

form an amorphous phase. Attempts to quantify the crystalline components using the Rietveld method resulted in values of metallic tungsten and W_2C of about 2 mass% each. The amounts of $M_{12}C$ and M_6C in the as-sprayed state were determined to be 14.2 and 5.6 mass%, respectively.

The low-magnification micrographs in Fig. 6(a) and (b) show the microstructures of the sample in the as-sprayed state and after thermal cycling, respectively. At this level, they show both the typical splat-like microstructure containing a certain amount of pores.

The high-magnification micrograph (BSE mode) presented in Fig. 7 shows the WC grains of about 1 μm in size embedded in the binder phase containing cobalt and different amounts of tungsten. The inhomogeneous distribution of tungsten causes the different contrast levels in the BSE micrograph.

Due to the repeated mention of the existence of W_2C in rims around WC grains in as-sprayed samples in the literature (Ref 4, 6, 9, 10, 12), special efforts were made to locate the W_2C by EDX elemental mapping, although as described above, XRD indicated the existence of minor

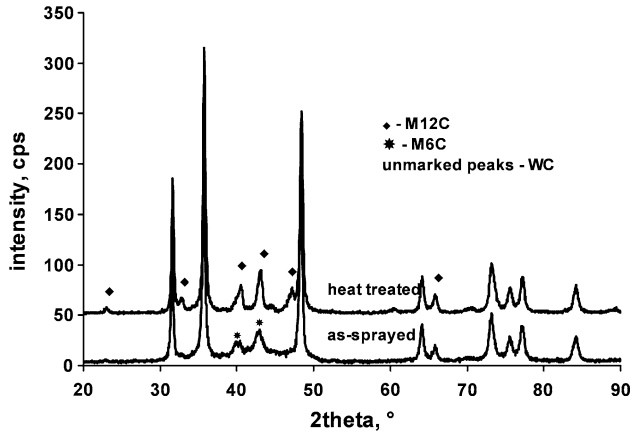

Fig. 5 XRD pattern of the as-sprayed state and after second thermal cycle in the thermoanalytical equipment

amounts only. Such W_2C rims around WC-grains were not detectable in the EDX mapping in the as-sprayed state (see Fig. 8). Areas with different brightness levels within

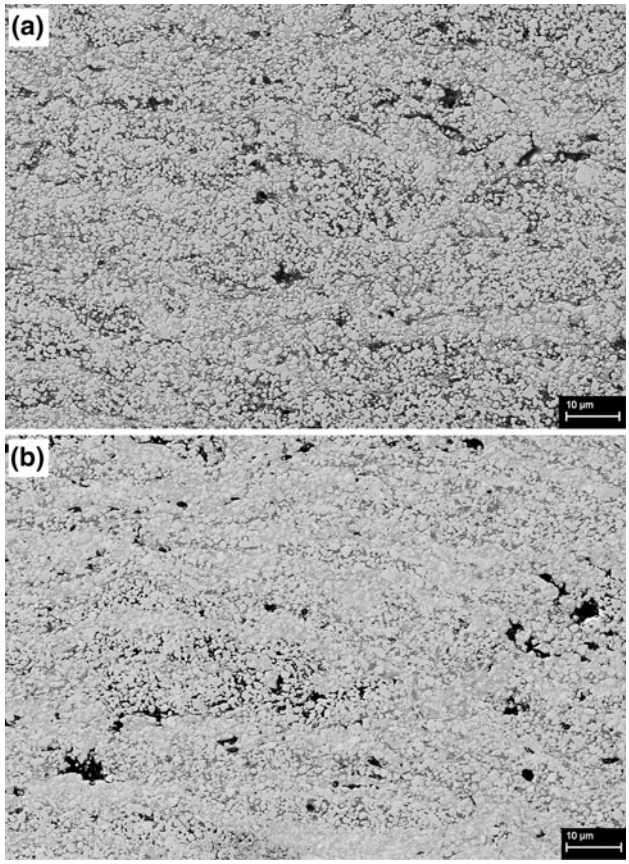

Fig. 6 Low-magnification micrograph (SE mode) of the sample in the as-sprayed state (a) and after thermal treatment (b)

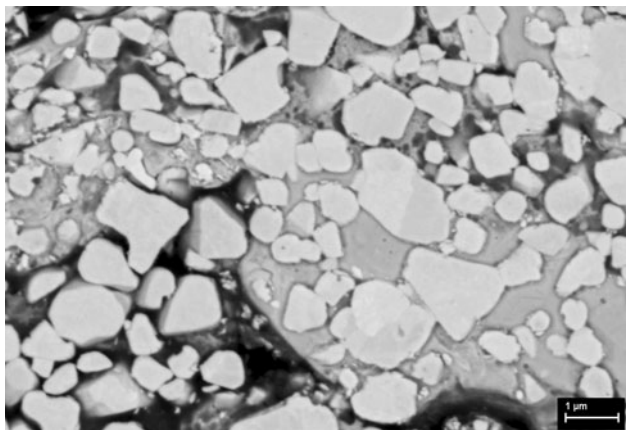

Fig. 7 High-magnification micrograph (BSE mode) of the sample in the as-sprayed state

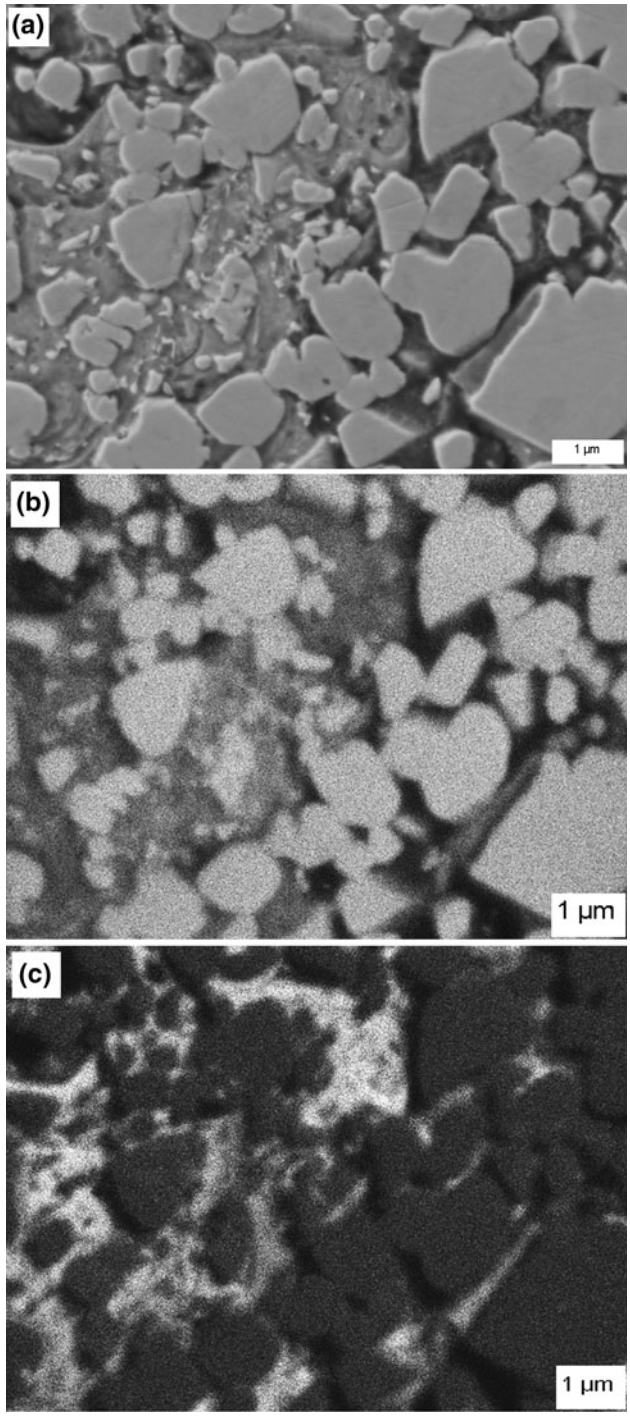

Fig. 8 SE micrograph (a) and elemental distribution of tungsten (b) and cobalt (c) in the EDX mapping of the sample in the as-sprayed state

the WC grains appearing in the micrograph in Fig. 7 result from different crystal orientations. Figure 9 shows the EDX mapping after the second thermal cycling.

In order to explain the microstructural changes in the first cycle, special efforts were directed to the study of the structure of the metallic binder phase. The high-resolution FESEM micrograph of the binder phase in Fig. 10 shows the binder phase in the as-sprayed state, being nanostructured or partially amorphous. During investigation of the matrix using an EBSD detector the crystal pattern (zone axes) of cobalt was detectable at some spots.

As shown in the x-ray diffraction pattern in Fig. 5 after thermal cycling the crystalline $M_{12}C$ phase content in-

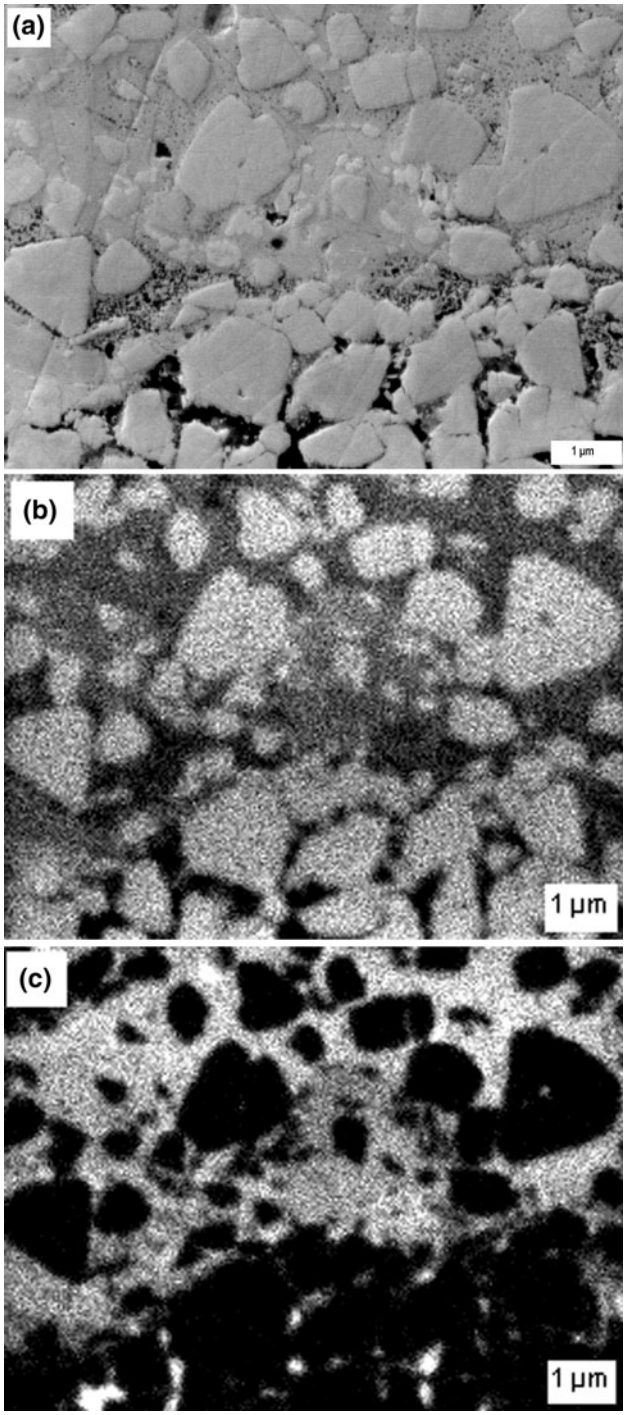

Fig. 9 SE micrograph (a) and elemental distribution of tungsten (b) and cobalt (c) in the EDX mapping of the sample after second thermal cycling

creased considerably. The Rietveld calculations indicated an amount of 19.4 mass% of $M_{12}C$ and 3.6 mass% of M_6C. The W_2C phase content was calculated to be 1.7 mass%. The high-resolution FESEM micrograph (Fig. 11) indicated a binder phase consisting of grains in a size range of 25 to 100 nm.

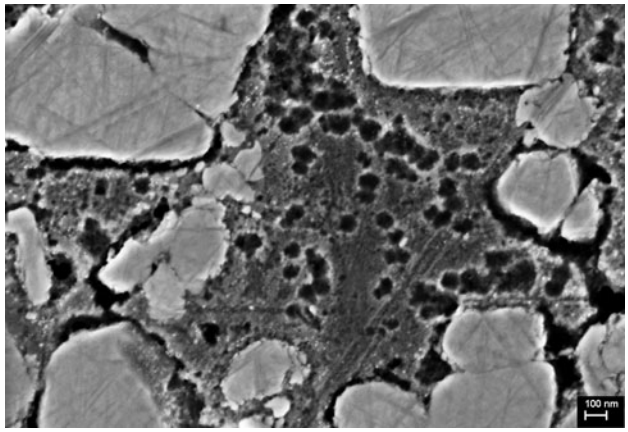

Fig. 10 Microstructure of binder phase of the as-sprayed sample (InLens detector)

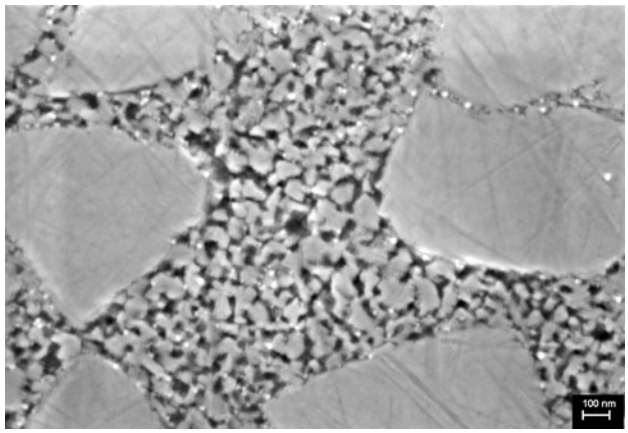

Fig. 11 Microstructure of binder phase of the sample after cycling (InLens-detector)

3.3 Comparison with XRD Measurements Performed for the As-Sprayed Sample

As mentioned above, the phase composition detected for the as-sprayed sample taken from the specimen for the thermoanalytical measurements was contrary to expectations. Although details of sample preparation for the XRD measurements are not given in the literature (Ref 6, 9, 10, 12), it can be proposed that in the majority of cases XRD patterns are obtained from as-sprayed coating surfaces without any finishing. Since the information is collected from a coating volume of less than 10 µm beneath the surface differences in phase composition might occur. For this reason comparison of the XRD patterns obtained from the as-sprayed surface and from one sample for thermoanalytical measurements was made. As shown in Fig. 12, the diffraction patterns exhibited remarkable differences, the pattern of the latter showing an increase in the amount of crystalline phases. For the pattern taken from the as-sprayed surface by the Rietveld method 3.8 mass% W_2C, 10.1 mass% $M_{12}C$, and 5.2 mass% M_6C were calculated.

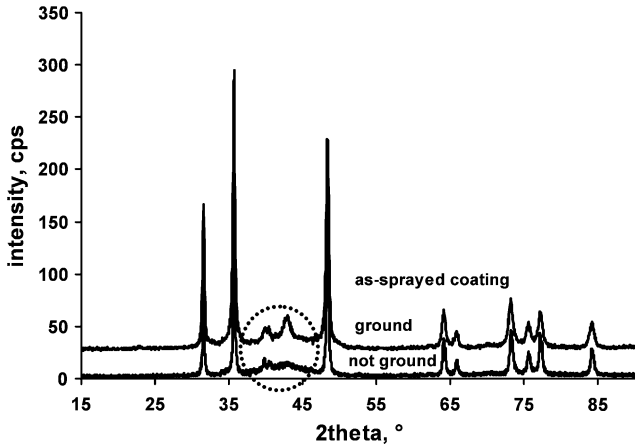

Fig. 12 XRD pattern of as-sprayed surface and thermoanalytical specimen

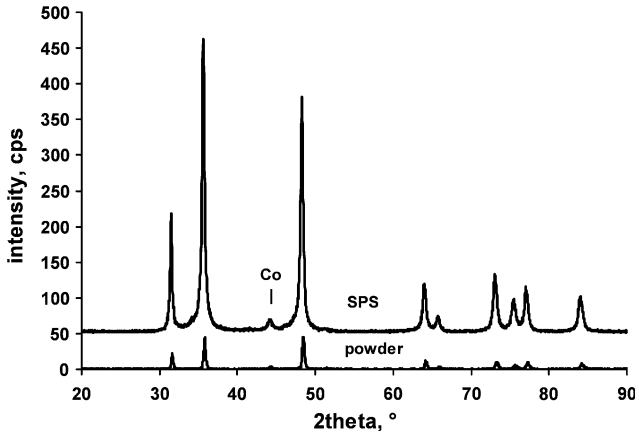

Fig. 13 XRD pattern of powder and SPS sample (all unmarked peaks = WC)

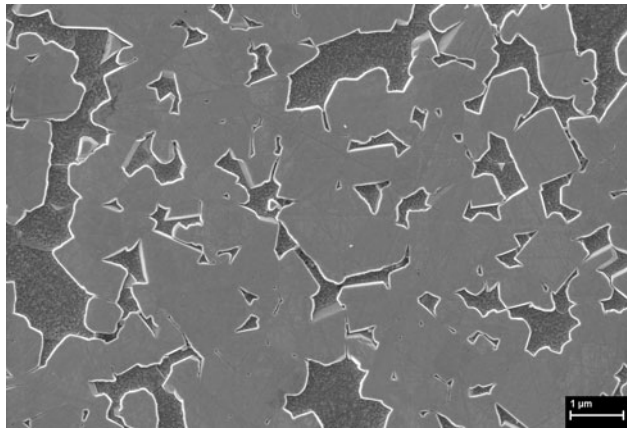

Fig. 14 Low-magnification micrograph of the SPS sample (InLens-detector)

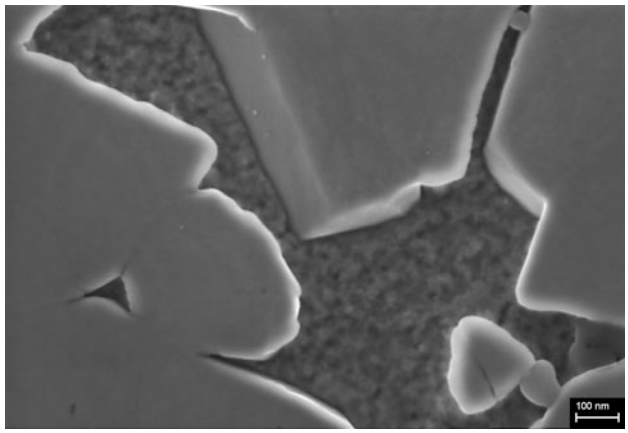

Fig. 15 Microstructure of the Co binder phase in the SPS sample (InLens-detector)

3.4 Microstructures and Phase Compositions of the Bulk Sample

In Fig. 13, the XRD patterns of the feedstock powder and the bulk sample prepared by SPS from the feedstock powder are compared. Both consisted of WC and cobalt only. Figure 14 shows the micrograph of the SPS sample. Despite the fact that the same feedstock powder was used in both the cases, the microstructure of the SPS sample was found to differ significantly from that of the coating (see Fig. 7) The bulk sample is characterized by the appearance of a skeleton of WC particles of size similar to that found in the coating. However, the WC particles in the thermal sprayed coatings are rounded due to the partial dissolution of WC during spraying.

The high-magnification FESEM micrograph in Fig. 15 shows that the cobalt binder phase consists of cobalt crystallites in a size range of 10 to 15 nm. The microstructure of the SPS sample is obtained through a much faster sintering process when compared with conventional sintering conditions and a temperature (1250 °C) below appearance of a melt. Therefore, the microstructure of the SPS sample may be assumed to be the best that can be obtained from this particular feedstock powder.

4. Discussion

The composition and microstructure of the feedstock powder are dramatically changed during the in-flight period and during coating formation. During the in-flight period there are physical processes such as dissolution of WC into the metallic binder matrix accompanied by chemical changes, carbon loss being the most important. Rapid cooling during coating formation leads to a non-equilibrium state of the composition. The FESEM investigations in this study showed that the metallic binder is predominantly in a nanocrystalline state (see Fig. 10).

The phases detected in the WC-17%Co coating in this study were different from the expectations and those described in the literature (Ref 4, 6, 9, 10, 12). W_2C and

metallic tungsten were found only in small amounts, whereas larger amounts of M_6C and $M_{12}C$ carbides were detected. Both W_2C and metallic tungsten are phases found in the nonequilibrium state of WC-Co coatings, while M_6C and $M_{12}C$ carbides are phases which are formed when the coating composition is moving in the direction of its equilibrium under the influence of heat. This indicates that the as-sprayed condition in this study is already closer to the equilibrium state than is commonly observed. Indeed, the deposition conditions of the samples in this study are different (higher heat inside the coating during deposition) from those usually applied due to the very high coating thickness of about 1.4 mm. Although not in all references who have observed the formation of W_2C rims (Ref 4, 6, 9, 10, 12) the coating thickness is given, it was or can be assumed as significantly thinner, leading to a faster cooling rate of the coating. This hypothesis is further supported by the differences in the phase composition measured for the as-sprayed coating surface, which cools down more rapidly, and those from the samples for thermoanalytical measurements machined from the inner structure of the coating.

The $M_{12}C$ grains located in the binder phase were seen to grow as a result of the heat treatment in the thermoanalytical investigations, which also caused an increase in the peak intensity in the XRD pattern. Due to carbon loss in the spray process the $M_{12}C$ phase was in equilibrium for the given coating composition in the W-C-Co system. Correspondingly, the bulk sample, prepared by SPS from the same feedstock powder, consisted of WC and metallic cobalt only.

The heat conductivity of a bulk WC-15%Co hardmetal is reported to be 60 W/mK (Ref 18). Therefore, the heat conductivity of the WC-17%Co coating determined in this study is about half that of the bulk material.

5. Conclusions

As indicated by the presence of $M_{12}C$ and M_6C, the phase composition of the WC-17%Co coating used in this study for thermoanalytical measurements was closer to the equilibrium state than is commonly described in the literature. Therefore, the phase composition detected in the WC-Co coating appeared to be sensitive to the heat regime of the coating during deposition. The metallic binder in the as-sprayed coating was predominantly in a nanocrystalline state. With one thermal cycle up to 700 °C, $M_{12}C$ crystal growth in the binder regions was observed. A heat conductivity ranging from 29.2 W/(mK) at 50 °C to 35.4 W/(mK) at 700 °C was determined.

Acknowledgments

This study was supported by the FhG Internal Programs under Grant No. WISA 816 442. The authors wish to thank Dr. Mathias Herrmann, IKTS Dresden, for performing the XRD Rietveld analysis.

References

1. R. Ahmed and M. Hadfield, Mechanisms of Fatigue Failure in Thermal Spray Coatings, *J. Thermal Spray Technol*, 2002, **11**(3), p 333-349
2. L.-M. Berger, J. Spatzier, J. Bretschneider, K. Lipp, and S. Thiele, Rolling Contact Fatigue of HVOF-Sprayed Hardmetal Coatings on Unhardened Substrates, *Thermal Spray Bull.*, 2009, **2**(2), p 133-140
3. L.-M. Berger, M. Woydt, S. Saaro, Reib-/Gleitverschleiß von thermisch gespritzten Hartmetallschichten (Sliding Wear of Thermally Sprayed Hardmetal Coatings), *Jahrbuch Oberflächentechnik*, R. Suchentrunk, Ed., Eugen G. Leuze Verlag, Bad Saulgau, 2007, p 242-267 (in German)
4. L.-M. Berger, Hardmetals as Thermal Spray Coatings, *Powder Met.*, 2007, **50**(3), p 205-214
5. M.E. Vinayo, F. Kassabji, J. Guyonnet, and P. Fauchais, Plasma Sprayed WC-Co Coatings: Influence of Spray Conditions (Atmospheric and Low Pressure Plasma Spraying) on the Crystal Structure, Porosity, and Hardness, *J. Vac. Sci. Technol.*, 1985, **3A**(6), p 2483-2489
6. J.M. Guilemany, J.M. de Paco, J. Nutting, and J.R. Miguel, Characterization of the W_2C Phase Formed during the High Velocity Oxygen Fuel Spraying of a WC +12%Co Powder, *Metal. Mater. Trans.*, 1999, **30A**(8), p 1913-1921
7. C.-J. Li, A. Ohmori, and Y. Harada, Effect of Powder Structure on the Structure of Thermally Sprayed WC-Co Coatings, *J. Mater. Sci.*, 1996, **31**(3), p 785-794
8. C.-J. Li, A. Ohmori, and Y. Harada, Formation of an Amorphous Phase in Thermally Sprayed WC-Co, *J. Thermal Spray Technol.*, 1996, **5**(1), p 69-73
9. C. Verdon, A. Karimi, and J.-L. Martin, A Study of High Velocity Oxy-Fuel Thermally Sprayed Tungsten Carbide Based Coatings. Part 1: Microstructures, *Mater. Sci. Eng.*, 1998, **A246**(1-2), p 11-24
10. R. Schwetzke and H. Kreye, Microstructure and Properties of Tungsten Carbide Coatings Sprayed with Various High-Velocity Oxygen Fuel Spray Systems, *J. Thermal Spray Technol.*, 1999, **8**(3), p 433-439
11. D.A. Stewart, P.H. Shipway, and D.G. McCartney, Influence of Heat Treatment on the Abrasive Wear Behaviour of HVOF Sprayed WC-Co Coatings, *Surf. Coat. Technol.*, 1998, **105**(1-2), p 13-24
12. D.A. Stewart, P.H. Shipway, and D.G. McCartney, Microstructural Evolution in Thermally Sprayed WC-Co Coatings: Comparison between Nanocomposite and Conventional Starting Powders, *Acta Mater.*, 2000, **48**(7), p 1593-1604
13. P. Vuoristo, K. Niemi, T. Mäntylä, L.-M. Berger, and M. Nebelung, Comparison of Different Hardmetal-Like Coatings Sprayed by Plasma and Detonation Gun Processes, *Advances in Thermal Spray Science and Technology*, C.C. Berndt and S. Sampath, Ed., ASM International, Houston, TX, 1995, p 309-315
14. J. Nerz, B. Kushner, and A. Rotolico, Microstructural Evaluation of Tungsten Carbide-Cobalt Coatings, *J. Thermal Spray Technol.*, 1992, **1**(2), p 147-152
15. S. Zimmermann, H. Keller, and G. Schwier, New Carbide Based Materials for HVOF Spraying, *Thermal Spray 2003: Advancing the Science and Applying the Technology*, C. Moreau and B. Marple, Ed., ASM International, Orlando, FL, 2003, p 227-232
16. L.-M. Berger, P. Vuoristo, T.Mäntylä, and W.Gruner, A Study of Oxidation Behaviour of WC-Co, Cr_3C_2-NiCr and TiC-Ni-based Materials in Thermal Spray Processes, *Thermal Spray: Meeting the Challenge of the 21st Century*, C. Coddet, Ed., May 25-29, 1998 (Nice, France), ASM International, 1998, p 75-82
17. L.-M. Berger, R. Zieris, and S. Saaro, Oxidation of HVOF-Sprayed Hardmetal Coatings, *Proc. Int. Thermal Spray Conference & Exhibition*, May 2-4, 2005 (Basel, Switzerland), DVS-Verlag, Düsseldorf, 2005, 8 p (CD)
18. H. Kolaska and W. Weith, Hartmetalle als Werkstoffe für Konstruktionsbauteile (Hardmetals as Materials for Construction Parts), *Metall*, 1995, **49**(2), p 104-111 (in German)